Chapter 4

Atlas-based organ & bone approximation for *ex-vivo* μMRI mouse data

A. Khmelinskii, M. Baiker, X. J. Chen, J. H. C. Reiber, R. M. Henkelman and B. P. F. Lelieveldt Proceedings of the 7th IEEE International Symposium on Biomedical Imaging: From Nano to Macro, Pages: 1197–1200 2010

Abstract

In this paper we propose a novel semi-automated atlas-based approach for organ and bone approximation for μMRI data of mice. Based on a set of 18 manually indicated landmarks at specific joint & bone locations, individual atlas bones (pelvis, limb bones and sternum) are mapped to the target in a first step and a sparse set of corresponding landmarks on a skin surface representation is determined in a second step. Subsequently, this sparse set on the skin is used to derive a dense set of correspondences relying on matching spectra of local geodesic distances. Finally, determined by the skin correspondence, a Thin-Plate-Spline (TPS) approximation of major organs (heart, lungs, liver, spleen, stomach, kidneys) is performed. The method was tested using 3 μMRI mouse datasets and the MOBY atlas. The performance of the organ approximation algorithm was estimated using manual segmentations of 6 organs for each MRI dataset and calculating Dice indices of organ-volume overlap for each dataset and the atlas. The obtained results indicate excellent fitting of heart and kidneys and moderate fitting of spleen, lungs, liver and stomach. These initial results are satisfactory and comparable to other organ mapping studies using different approaches and μCT mouse data.

4.1 Introduction

In pre-clinical research, whole-body small animal (mice and rats) imaging is widely used for the *in vivo* visualization of functional and anatomical information to study cancer, neurological and cardiovascular diseases and help with a faster development of new drugs. Structural imaging modalities such as MRI, CT and ultrasound provide detailed depictions of anatomy; PET, SPECT, and specialized MRI protocols add functional information. In addition, optical imaging modalities, such as BLI and near-infrared (NIR) microscopy offer a high sensitivity in visualizing molecular processes *in vivo*. In combination, these modalities enable the visualization of the cellular function and the follow-up of molecular processes in living organisms without sacrificing them.

However, whole-body imaging creates a large amount of data and there is an urgent need to effectively combine, organize, analyze and quantify all this data to help look for differences between wild type and mutant mice rapidly and with minimal human intervention. This is a complicated task, since an animal body is a complex system with many rigid (bones), non-rigid (organs) structures and articulated parts [1] leading to shape and postural variability in follow-up and cross-sectional studies.

For different imaging modalities several approaches were proposed to solve this problem of fitting whole-body small animal data to a common reference. Joshi *et al.* [2] proposed a method for fitting an elastically deformable mouse atlas to surface topographic range data acquired by an optical system; this method does not incorporate the extremities. Wildeman *et al.* [3] proposed a 2D/3D registration of μCT data to multi-view photographs based on a 3D distance map combining optical data with CT. Baiker *et al.* presented a fully automated skeleton registration and organ approximation method using an articulated whole-body atlas in μCT mouse data [1]. This method exploits the high contrast of bone to automate the registration process of the skeleton model and the subsequent organ

approximation; the reason for this is the fact that optical and CT lack soft tissue contrast for most abdominal organs. In this paper, we investigate the generalization of this method towards application in μMRI data. This type of data provides greater contrast between the different soft tissues of the body, but poorer bone contrast than CT data. We present a semi-automated atlas-based bone and organ approximation method for μMRI data. 18 joint landmarks are manually determined and together with surface representations of the bones and the skin, individual atlas bones are mapped to the target based on the joint correspondences and the organs are mapped using TPS approximation as reported earlier in [1]. Given the complexity of this type of data, the work described in this paper is a first step towards a more automated whole-body atlas-based bone and organ mapping in μMRI mouse data.

The contributions of this paper are twofold:

(i) we present a novel semi-automated organ approximation method for μMRI mouse data that considerably reduces the required user effort compared to manual segmentation

(ii) the presented method includes the limbs and provides a shape approximation of the bones in MR data. The user interaction mechanism to identify the joints is guided by anatomically realistic kinematic constraints imposed by the atlas

4.2 Materials and methods

4.2.1 MOBY atlas

In this work the MOBY mouse atlas was used as the anatomical reference (Figure 1.(a)). Using a *C57BL/6,* 15 weeks old male mouse, Segars *et al.* [4] generated a realistic 4D digital mouse phantom based on high-resolution 3D MRI data from Duke University. The organs of this atlas are represented using non-uniform rational bspline (NURBS) surfaces, which are widely used in 3D computer graphics. For bone approximation we used an articulated version of the MOBY skeleton [1], where all major bones or bone compounds like the paws were separately labeled and joint locations and types were defined. See Figure 4.1.(b).

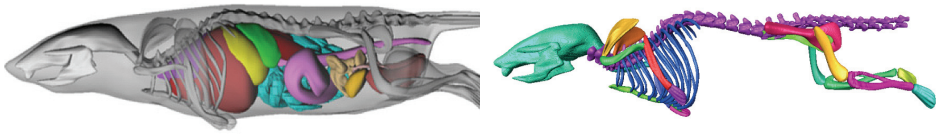

(a) (b)

Figure 4.1 MOBY mouse atlas: (a)—Original skeleton + organs + skin. (b)—Articulated skeleton

4.2.2 µMRI data acquisition and manual organ segmentation for evaluation

Sixteen *C3H* mice were perfusion fixed with formalin and 10 mM Magnevist with ultrasound guidance [5]. Imaging was performed on a 7–T magnet with a four-channel VarianINOVA™ console (Varian Inc., Palo Alto, CA) multiplexed to 16 coils for parallel imaging. A spin echo sequence was used: TR/TE = 650/15ms and (100 µm)^3 voxels with an imaging time of 13h[1]. In this work a subset of 3 mice was used.

To validate and evaluate the performance of the method presented in this paper, six organs (liver, heart, kidneys, lungs, stomach and spleen) were manually segmented by an expert in all three mice using the Amira™ software [6].

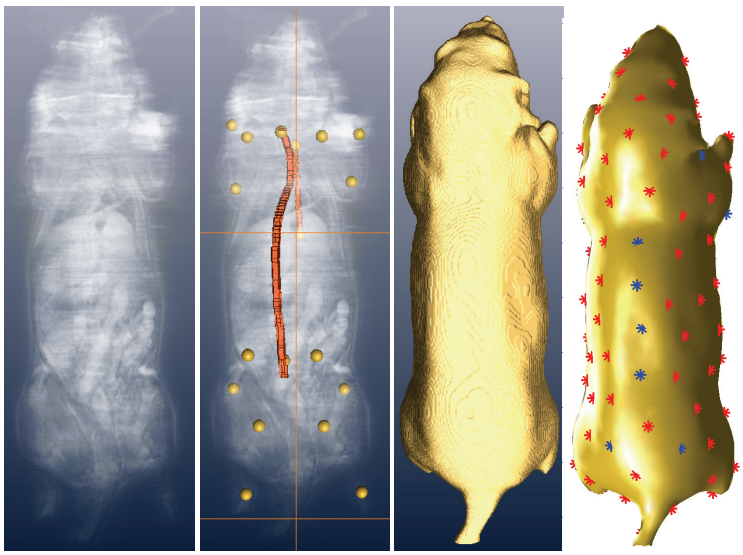

(a) (b) (c) (d)

Figure 4.2 Landmark extraction: (a)—Original data. (b)—Manual landmarks: 2 knee joints, 2 hip joints, posterior and anterior extremities of the *sternum*, middle of the atlas vertebra, middle of the last *lumbar vertebra* and the correspondent inner surface of the *columna vertebralis*, 2 elbow joints, 2 shoulder joints, 2 ankle joints, 2 wrist joints, right and left anterior *pelvis* extremities. (c)—Mouse skin. (d)—Initial (blue) and dense (red) sets of skin correspondences used for TPS organ approximation

4.2.3 Manual landmark selection

Using the Amira™ software and guided by an anatomical text book [7] the following 18 joint and bone landmarks were manually extracted in all 3 mouse datasets: 2 *femur/tibia-fibula*—knee joints, 2 *femur/pelvis*—hip joints, posterior and anterior extremities of the *sternum,* right and left anterior pelvis extremities, middle of the *atlas vertebra,* middle of the last *lumbar vertebra,* 2 *humerus/ulna-radius*—elbow joints, 2 *humerus/scapula*—shoulder joints, 2 *tibia-fibula/pes*—ankle joints and 2 *ulna-radius/manus*—wrist joints. Between the middle of the *atlas vertebra* and middle of the last *lumbar vertebra* respectively, the inner

[1] All animal protocols were approved by the Hospital for Sick Children Animal Care Committee

surface of the *columna vertebralis* was extracted. This whole step takes about 1 hour to execute and the final result can be seen in Figure 4.2.(b).

4.2.4 Joint identification

As mentioned above, the joints have to be indicated manually. To facilitate this procedure, we developed a method for automated joint identification. The expert does not have to follow a strict identification protocol every time but is free to indicate the joints in arbitrary order. Using the atlas joint locations, anatomically realistic bone dimensions, anatomically realistic Degrees of Freedom (DoFs) for each joint and a hierarchical anatomical model of the skeleton (please refer to [1] for details) all joints can be labeled. After identification of a hip joint, the more distal joints are identified by searching candidates that lie within a minimum/maximum Euclidean distance of the length of the atlas upper hind limb ± 15% as we consider a bone length in the atlas ± 15% as anatomically realistic variation. In addition, the knee joint has to lie within an anatomically realistic solid angle according to the properties of the hip, which is a ball joint. In most cases, this clearly identifies the knee joint but sometimes there can be two candidates, if the ankle joint is in approximately the same distance from the hip and the knee. In such a case, all possible hip, knee, ankle constellations have to be tested for plausibility.

4.2.5 Skin extraction

For each mouse dataset, triangular surface meshes of the skin were automatically extracted using the marching-cubes algorithm [8] after performing a chain of Gaussian smoothing(σ=5)-thresholding-morphological filtering on the original data to remove noise, artifacts and organ regions. See Figure 4.2.(c). This task and all the included steps was automatically executed using MeVisLab™ software [9]. Skin surface was simplified to approximately 2000 vertices using the QSlim method by Garland *et al.* [10]. Note that the extracted isosurface is not perfect, since it does not cover the mouse body to its full extent: the *pes* and the *manus* were left out. However, those are not necessary for the proposed method.

4.2.6 µMRI data organ approximation

Based on a subset of 14 of the manually selected landmarks (the wrist and the ankle joints are not used for mapping the organs) and four additional landmarks, derived using the manual spine approximation, a sparse set of 16 corresponding skin landmarks is derived. Since at many locations in the animal body, skin is very close to the skeleton, we simply take the skin vertex with the smallest Euclidean distance from each joint. Note that the initial set of correspondences was established for the atlas skin in the same manner as for the target. However, this has to be done only once. Starting from this sparse set of correspondences, a dense set of 99 correspondences on the skin is determined. To this end we use a method presented previously in [1]. In short, the method searches for new correspondences in the local neighborhood of the already established correspondences. To this end, local geodesic spectra for candidate vertices on the skin surface are determined and compared to geodesic spectra that are available for all atlas skin vertices. The pair of vertices in the target and the atlas that yields the highest geodesic spectrum similarity is added to the list of correspondences and so on. In several iterations,

vertices from all over the skin surface are added. Figure 4.2.(d) shows the initial set and the final set of correspondences on the target skin. Using the skin correspondences, the organs can be warped from the atlas domain to the subject domain. In its original form *i.e.,* if used as an interpolant, the TPS does force landmarks in the source domain to fit landmarks in the target domain exactly. However, due to the discretization of the skin surface, in general small spatial errors may occur and this can cause local distortions of the mapping. A remedy is to allow small landmark localization errors and relax the constraint of interpolation towards approximation (thin-plate smoothing spline [11]).

4.2.7 Rule-based μMRI data bone approximation

For mapping individual bones from the atlas to the target domain, we employ a similarity transformation model with 7 DoFs to account for translation and rotation as well as for differences in bone size. This means that in 3*D*, three corresponding points have to be known for each bone. Since all joint locations are available, most of the DoFs for each element can be resolved by mapping the joint in the atlas to the corresponding joint in the target. Taking the right upper hind limb (femur) for instance this means that the right atlas hip is mapped to the right target hip first, resolving the three translation parameters. Second, the right atlas knee is mapped to the right target knee, resolving two rotations and the scaling parameter. The third rotation parameter, the rotation with respect to the longitudinal axis of the bone, cannot be resolved using the hip and the knee joint only. However we can address this problem because the right ankle joint is available, knowing that the knee joint is a hinge joint. Since this joint type allows only one rotation of one bone with respect to the other, a longitudinal bone rotation can be resolved. Both knees as well as the elbows are hinge joints and therefore the transformation parameters for all eight limb bones can be determined uniquely. For the pelvis, four and therefore enough landmarks are available to derive the mapping transformation.

4.3 Experimental results

The validation of the organ approximation method was done using the 3 datasets with manually segmented organs described in 4.2. To have a quantitative estimation of the organ approximation method performance, the Dice index of volume overlap for 6 organs (liver, heart, kidneys, lungs, stomach and spleen) was calculated for the 3 mice and the MOBY atlas:

$$\text{Dice index} = \frac{2\left|V_s \cap V_a\right|}{\left|V_s\right| + \left|V_a\right|} \tag{1}$$

where *Vs* and *Va* correspond to the subject and atlas volumes respectively.

Examples of the organ & bone approximation and the manually segmented mice are shown in Figures 4.3, 4.4 and quantitative results are presented in Table 4.1.

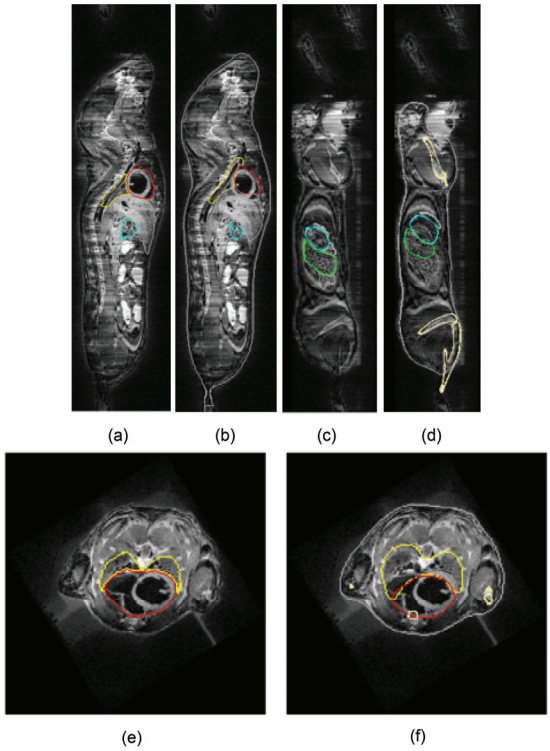

Figure 4.3 Organ & Bone approximation results for μMRI mouse data: (a), (c) & (e)—Manual Organ segmentation. (b), (d) & (f)—Organ & Bone Approximation results. Coronal & Sagittal planes respectively. *yellow*—lungs, *red*—heart, *green*—spleen, *cyan*—stomach, *cream*—bone, *grey*—skin, *white*—liver

The organ approximation method gives excellent fitting results for the heart and kidneys with maximum Dice indices 0.80 and 0.72 respectively. The worst result is obtained for the spleen with the dice index varying between 0.25 and 0.36. For the remaining organs—liver, lungs, stomach the fitting is of moderate success and the dice index is within the 0.39–0.68 interval. These results are comparable with the results obtained by Baiker *et al.* in [12] for μCT data. The heart and liver Dice indices are similar for both methods, whereas the method presented here is a little bit better with respect to the kidneys. However the lung approximation results in [12] are much better which can be explained by the fact that in μCT data this organ could be automatically extracted and registered to the atlas.

Regarding the bone approximation, although we present no quantitative assessment, in Figures 4.3.(d)., (f). and 4.4 it is visible that the obtained results are of moderate success. However there are visible misalignments, especially with respect to the pelvis and this can be explained by imprecisions in manual joint & bone landmark selection process.

The entire organ & bone approximation algorithm was implemented in MATLAB *R2008b*™ and took approximately 3 minutes of runtime in a 2.40*GHz* Intel Quad Core™ with 4*GB* of RAM, Windows™ PC.

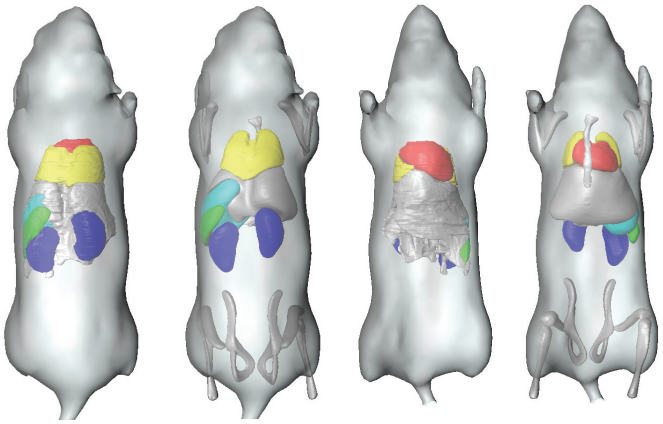

(a) (b) (c) (d)

Figure 4.4 Manual Organ segmentation: (a) & (c). Bone and Organ Approximation: (b) & (d). Top & Bottom views respectively

4.4 Discussion and conclusion

In this paper a semi-automated atlas-based organ approximation method for μMRI mouse data is proposed. A manually extracted set of joint & bone landmarks and the automatically extracted skin are used to determine skin correspondences, which in turn are used for a TPS approximation of major organs (heart, lungs, liver, spleen, stomach, kidneys).

For some organs, the obtained results are generally satisfactory and similar to the manual segmentations (heart, kidneys, liver), while for other organs the atlas approximations are more variable. Especially for organs with inherent shape variability such as the stomach and spleen, errors were larger. Also, inaccuracies in manual landmark selection and imperfections in the skin extraction may contribute to these misalignments. In these cases, further manual correction of the contours is required. The computation time of the organ approximation method is very low and though the 18 manual landmark selection is a tedious process taking around 1 hour to perform it is much faster than the manual organ segmentation which takes around 10 hours to execute (for the 6 organs tested). This work represents a first step towards a more automated atlas-based skeleton and organ mapping. Also, a comparison with results obtained with other whole-body atlases like the Digimouse [13] is ongoing.

	Mouse 1			Mouse 2			Mouse 3			[12]
	V_s(mm³)	V_a(mm³)	Dice	V_s(mm³)	V_a(mm³)	Dice	V_s(mm³)	V_a(mm³)	Dice	Dice
Heart	292.62	227.16	0.65	282.36	241.83	0.80	292.56	202.19	0.74	0.81
Spleen	90.79	64.38	0.25	101.69	77.57	0.36	102.65	76.88	0.30	N/A
Lungs	421.15	392.78	0.39	429.74	437.26	0.56	344.55	362.38	0.44	0.70
Kidneys	264.57	268.10	0.43	301.28	268.94	0.72	305.68	231.27	0.72	0.48
Liver	1131.77	1776.11	0.63	1087.54	1939.77	0.68	1484.82	1551.95	0.63	0.73
Stomach	323.80	317.00	0.56	354.30	385.18	0.64	295.24	361.89	0.62	N/A

Table 4.1 Organ approximation results for 3 μMRI mouse datasets: dice indices for 6 major organs—heart, spleen, lungs, kidneys, liver, stomach. Last column: comparison with the automatic organ approximation results obtained by Baiker *et al.* [12] for μCT mouse data. *Vs*=subject volume, *Va*=atlas volume

Acknowledgments

The authors gratefully acknowledge Paul Segars for providing the MOBY mouse atlas and Yu-Qing Zhou and Jonathan Bishop for whole-mouse preparation and image acquisition, respectively.

References

[1]. Baiker M., Milles J., Dijkstra J. *et al. Atlas-based whole-body segmentation of mice from low-contrast micro-CT data* Med Image Anal 14(6): 723–737 2010

[2]. Joshi A. A., Chaudhari A. J., Li C. *et al. Posture matching and elastic registration of a mouse atlas to surface topography range data* Proc IEEE Intl Symp Biomed Imaging 366–269 2009

[3]. Wildeman M. H., Baiker M., Reiber J. H. C. *et al. 2D/3D registration of micro-CT data to multi-view photographs based on a 3D distance map* Proc IEEE Intl Symp Biomed Imaging 987–990 2009

[4]. Segars W. P., Tsui B. M. W., Frey E. C. *et al. Development of a 4-D digital mouse phantom for molecular imaging research* Mol Imaging Biol 6(3): 149–159 2004

[5]. Zhou Y. Q., Davidson L., Henkelman R. M. *et al. Ultrasound-guided left-ventricular catheterization: a novel method of whole mouse perfusion for microimaging* Lab Invest 84(3): 385–389 2004

[6]. http://www.amira.com

[7]. Bab I., Hajbi-Yonissi C., Gabet Y. *et al. Micro-Tomographic Atlas of the Mouse Skeleton* Springer 2007

[8]. Lorensen W. E. and Cline H. E. *Marching cubes: A high resolution 3D surface construction algorithm* Proc of the 14th Annual Conf on Computer Graphics and Interactive Techniques 163–169 1987

[9]. http://www.mevislab.de

[10]. Garland M and Shaffer E. *A multiphase approach to efficient surface simplification* Proc Conf on Visualization 117–124 2002

[11]. Wahba G. *Spline models for observational data*, SIAM ISBN-13: 978-0898712445 1990

[12]. Baiker M., Dijkstra J., Que I. *et al. Organ approximation in μCT data with low soft tissue contrast using an articulated whole-body atlas* Proc IEEE Intl Symp on Biomedical Imaging 1267–1270 2008

[13]. Dogdas B., Stout D., Chatziioannou A. *et al. Digimouse: a 3D whole body mouse atlas from CT and cryosection data* Phys Med Biol 52(3): 577–587 2007